

Atomic structure of the (Al,Si)CuFe cubic approximant phase

Frédéric Puyraimond,^a Marianne Quiquandon,^a Denis Gratias,^{a*} Monique Tillard,^b Claude Belin,^b Annick Quivy^c and Yvonne Calvayrac^c^aLEM-CNRS/ONERA, BP 72, 29 Avenue de la Division Leclerc, 92322 Châtillon CEDEX, France, ^bLAMMI/Université Montpellier II, 2 place Eugène Bataillon, 34095 Montpellier CEDEX 5, France, and ^cCECM/CNRS, 15 rue Georges Urbain, 94407 Vitry CEDEX, France. Correspondence e-mail: gratias@onera.fr

The structure of the α -(Al,Si)CuFe approximant phase is determined by a single-crystal X-ray diffraction study and compared to the ideal structure obtained by the perpendicular shear method of the parent icosahedral phase. It is shown that the local environments (typical atomic clusters) of the two phases are similar and expand significantly farther than the size of the unit cell of the approximant. The orbit Al(2) issuing from the theoretical icosahedral model corresponding to the inner dodecahedron of the Mackay-type cluster is not found in the approximant and is replaced by a partially occupied inner icosahedron with an unusually large Debye–Waller factor.

© 2002 International Union of Crystallography
Printed in Great Britain – all rights reserved

1. Introduction

This paper deals with the atomic structure determination of the α -(Al,Si)CuFe phase that is the simplest periodic approximant of the parent *F*-type icosahedral phase of the (Al,Cu,Fe) system. This phase of nominal composition $\text{Al}_{55}\text{Si}_7\text{Cu}_{25.5}\text{Fe}_{12.5}$ is a cubic $Pm\bar{3}$ structure with a lattice parameter $a = 1.2312(2)$ nm. It has been recognized as the 1/1 cubic approximant of *i*-AlCuFe with respect to both its geometry and its physical properties, which are indeed very similar to those of the parent icosahedral phase (Quivy *et al.*, 1996). Complementary to the recent study of Yamada *et al.* (1999), the goal of the present work (see also Puyraimond *et al.*, 2001) is to establish the details of the structural similarities between the α and icosahedral phases in the framework of the perpendicular shear technique introduced in the early 1990's by Jarić & Qiu (1990) for deciphering the average atomic structure of the quasicrystal from the knowledge of the approximant(s).

The paper is organized in two main parts. The first one is devoted to the description of the experimental conditions of the preparation of α -(Al,Si)CuFe single crystals, the X-ray data collection, the refinement technique and a short analysis of the refined structure in comparison with the previous results of Yamada *et al.* (1999). The second part deals with the modeling of the cubic phase using the shear method in 6D space. There, we present the basic 6D model of the *i*-AlCuFe phase with its main atomic clusters and show how the typical atomic clusters are expected to connect in the cubic phase. We finally discuss the characteristics of the refined structure in the framework of the ideal parent quasicrystalline phase and give some hints of how to slightly modify the quasicrystal model to

take into account the few discrepancies between the model and the diffraction results revealed in the present study.

2. Structure analysis of the α -(Al,Si)CuFe phase

2.1. Experimental conditions

An alloy of nominal composition $\text{Al}_{55}\text{Si}_7\text{Cu}_{25.5}\text{Fe}_{12.5}$ was prepared from the pure elements (Al 99.99, Si 99.999, Cu 99.999, Fe 99.99%) by induction melting. The entire ingot was remelted by induction heating in a silica nozzle and rapidly quenched by planar flow casting on a rotating copper wheel, under a pure helium atmosphere. The flakes were subsequently annealed over 11 days in an alumina crucible at 1068 K. At this temperature, the alloy is partially melted and large single crystals of the α -(Al,Si)CuFe phase (which can reach one millimetre in size) grow in the liquid. Single crystals are eventually mechanically extracted from the matrix and carefully crushed into smaller parts suitable for X-ray investigations. Several crystalline pieces were selected under an optical microscope and checked for singularity by preliminary oscillation and Weissenberg diffraction techniques. The crystals display cubic symmetry and no extinction condition was observed. The best single crystal of dimension $0.18 \times 0.10 \times 0.07$ mm was chosen for data collection at room temperature on an Enraf–Nonius CAD-4 automatic diffractometer using monochromatic Mo $K\alpha$ radiation ($\lambda = 0.71069$ Å). Accurate lattice parameters were determined [$a = 1.2312(2)$ nm] by least-squares refinements of the angular positions of 25 reflections collected and automatically centered on the diffractometer. Profile analysis of a few angle reflections indicated that $\omega - \theta$ scans were the most appro-

Table 1

Structure of the (1/1) approximant of the α -(Al,Si)CuFe phase resulting from the refinement process performed with the *SHELX97* program on the diffraction data.

The last column represents the Debye–Waller factor B_{eq} in \AA^2 . The starting structure is obtained by the perpendicular shear method with a lock-in point at the even nodes of the 6D *F* lattice as discussed in the text.

Atom	Wyckoff position	Occupancy	<i>x</i>	<i>y</i>	<i>z</i>	B_{eq} (\AA^2)
Fe(1)	1(<i>a</i>)	1	0	0	0	1.1 (1)
Al(2)	12(<i>j</i>)	10.7	0	0.098 (1)	0.1635 (9)	13.9 (7)
Cu/Al(3)	24(<i>l</i>)	17.1/6.9	0.1848 (1)	0.1172 (1)	0.2982 (1)	1.27 (3)
Cu/Al(4)	6(<i>e</i>)	4.25/1.75	0	0	0.3741 (3)	1.50 (7)
Fe(5)	12(<i>m</i>)	12	0	0.1987 (1)	0.3251 (1)	0.78 (3)
Al/Fe(6)	12(<i>k</i>)	10.3/1.7	0.6656 (2)	0.5	0.3986 (2)	0.57 (6)
Al(7)	24(<i>l</i>)	24	0.1912 (2)	0.3100 (1)	0.3846 (2)	0.51 (4)
Al(8)	6(<i>h</i>)	6	0.1149 (4)	0.5	0.5	0.24 (7)
Cu/Al(9)	12(<i>k</i>)	9.6/2.4	0.1805 (1)	0.5	0.3023 (1)	0.53 (4)
Cu(10)	6(<i>g</i>)	6	0	0.3113 (2)	0.5	0.76 (4)
Al/Fe(11)	12(<i>m</i>)	11.6/0.4	0	0.5998 (2)	0.3165 (3)	0.64 (8)
Al/Fe(12)	12(<i>k</i>)	11.6/0.4	0.1115 (2)	0.1263 (2)	0.5	0.78 (7)

Table 2

Comparison of the refined structures of the (1/1) approximant of the α -(Al,Si)CuFe phase between the results presented in this paper and those of Yamada *et al.* (1998).

The atomic species *M* corresponds to a mixture $M = 89 \text{ at.}\% \text{Al}/11 \text{ at.}\% \text{Si}$. The electron density of each Wyckoff position is given by the product of the atomic number *Z* of the atom(s) with the corresponding occupancy factor(s).

Wyckoff	Present results			Yamada <i>et al.</i> (1998)		
	Atom	Occupancy	Local electron density	Atom	Occupancy	Local electron density
1(<i>a</i>)	Fe(1)	1	26	Cu(1)	0.89	25.81
12(<i>j</i>)	Al(2)	10.7	139.1	<i>M</i> (2)	4.68	61.35
12(<i>j</i>)				<i>M</i> (2 _{<i>a</i>})	2.16	28.32
8(<i>i</i>)				<i>M</i> (2 _{<i>b</i>})	1.28	16.78
6(<i>e</i>)				<i>M</i> (2 _{<i>c</i>})	1.26	16.52
24(<i>l</i>)	Cu/Al(3)	17.1/6.9	585.6	Fe/ <i>M</i> (3)	20.16/3.84	574.5
6(<i>e</i>)	Cu/Al(4)	4.25/1.75	146	Cu/ <i>M</i> (4)	4.08/1.92	143.49
12(<i>m</i>)	Fe(5)	12	312	Cu/H(5)	9.24/2.76	304.14
12(<i>k</i>)	Al/Fe(6)	10.3/1.7	178.1	<i>M</i> /Cu(6)	10.08/1.92	187.83
24(<i>l</i>)	Al(7)	24	312	H(7)	24	314.64
6(<i>h</i>)	Al(8)	6	78	H/Cu(8)	5.58/0.42	85.33
12(<i>k</i>)	Cu/Al(9)	9.6/2.4	309.6	Cu/ <i>M</i> (9)	10.32/1.68	321.30
6(<i>g</i>)	Cu(10)	6	174	Cu/H(10)	5.46/0.54	165.42
12(<i>m</i>)	Al/Fe(11)	11.6/0.4	161.2	<i>M</i> /Cu(11)	11.64/0.36	163.04
12(<i>k</i>)	Al/Fe(12)	11.6/0.4	161.2	<i>M</i> /Cu(12)	11.52/0.48	164.95

priate. 3093 reflections were measured in the *hkl* octant ($0 \leq h, k, l \leq 17$) of the cubic cell in the range $2 \leq \theta \leq 30^\circ$. During data collection, intensities of three standard reflections were checked every hour without any significant fluctuation. Data were first corrected for background and for Lorentz–polarization effects, then a numerical absorption correction was applied ($\mu = 13.7 \text{ mm}^{-1}$, transmission factors from 0.464 to 0.320) using the procedure provided by *SHELX76* (Sheldrick, 1992; Sheldrick *et al.*, 1993). Equivalent reflections, according to the *Pm3* space-group symmetry, were averaged to $R_{\text{int}} = 4.15\%$. The final data set consists of 957 reflections of which 585 verify the $I \geq 2\sigma(I)$ condition.

2.2. Structure refinement and description

All our attempts to solve the structure *ex nihilo* with direct methods using *SHELXS* or *SHELXS97* (Sheldrick, 1992; Sheldrick *et al.*, 1993) have been unsuccessful. The structure

was eventually solved starting from the theoretical approximant obtained by the shear method locked-in at the even nodes of the 6D model. This will be discussed in §3. Refinements by full-matrix least squares were carried out using the program *SHELXL97* (Sheldrick, 1992; Sheldrick *et al.*, 1993). Atomic positions and isotropic thermal parameters for all atoms were refined before the occupancy factors. The final structure is given in Table 1.

During the refinement process, if one position appears to be incompletely filled, then its site occupation factor is freed but the fractional occupation factors are constrained to sum up to unity. One can notice in Table 1 that six atomic sites are considered with mixed occupation by different chemical species (chemical disorder), these positions are then refined. Finally, 76 parameters were refined to agreement factors $R_1 = 4.65$ and $wR_2 = 12.06\%$ with a goodness of fit *S* of 1.053 for 957 reflections. The reconstructed Fourier electron difference map indicates that the residual electron density varies

randomly between 1.44 and -1.27 e \AA^{-3} . The refined stoichiometry $(\text{Al,Si})_{61.8}\text{Cu}_{25.49}\text{Fe}_{11.32}$ agrees fairly well with the nominal composition $\text{Al}_{55}\text{Si}_7\text{Cu}_{25.5}\text{Fe}_{12.5}$. There are 137.7 atoms per unit cell of α -(Al,Si)CuFe (to be compared with 138 atoms per unit cell in α -AlMnSi).

As shown in Table 2, our results are in good agreement with those of Yamada *et al.* (1999) with resulting composition $(\text{Al,Si})_{60.85}\text{Cu}_{24.29}\text{Fe}_{14.86}$ obtained by Rietvelt refinement [program *RIETAN* (Izumi & Ikeda, 2000)] on powdered X-ray diffraction where the α -AlMnSi phase has been used as the starting structural model (Hiraga *et al.*, 1997; Sugiyama *et al.*, 1998; Yamada *et al.*, 1998, 1999). We observe that both structures are described with the same kind of Wyckoff positions [with the exception of the Al(2) position that will be discussed in the second part] although both the refinement processes and the initial structures were significantly different.

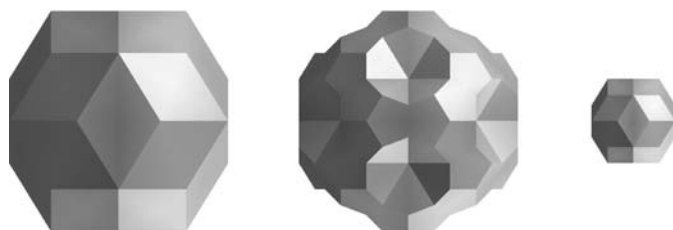


Figure 1
From left to right: the three main atomic surfaces in \mathbf{E}_{\perp} of the KGE model located respectively at n , n' and bc .

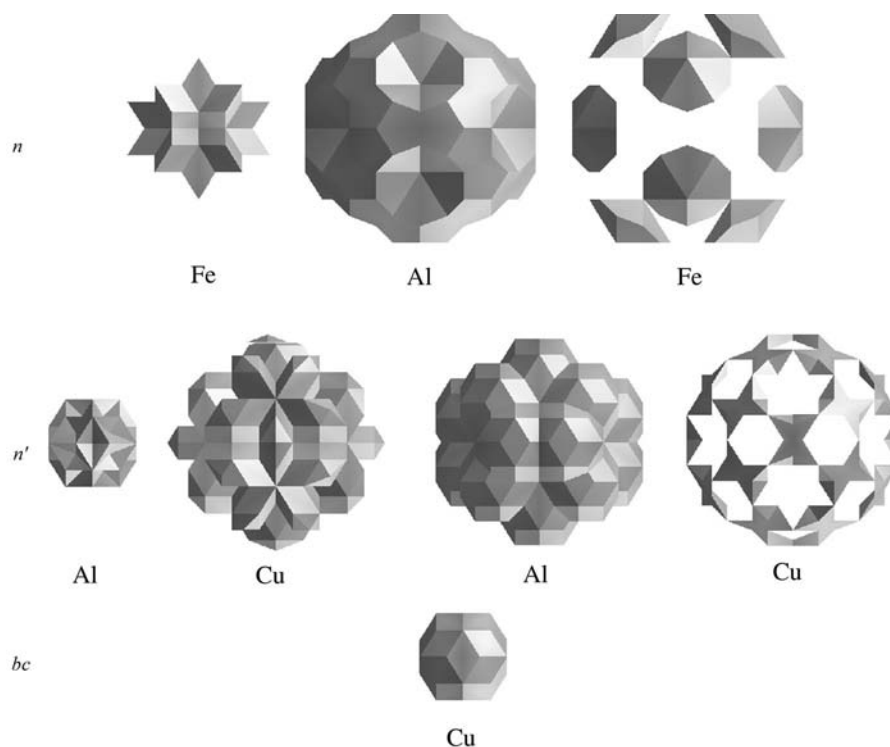


Figure 2
Atomic species distribution of Al, Cu and Fe on the three main surfaces of Fig. 1 as proposed by Katz & Gratias (1995) and modified by Elser (1996). This decoration has been shown to give satisfactory results with respect to composition, density and available diffraction data of the AlCuFe icosahedral phase.

The main differences between the two studies are the kind of atomic species that are attributed to the various Wyckoff positions. These differences are unavoidable using X-rays where the actual measurement involves the electron density: calculating the average electron density, $\sum v_i Z_i$ for each Wyckoff position, where i is the atomic species, Z_i its atomic number and v_i its occupancy factor, we observe that both structures give qualitatively the same local electron density. More generally, any atomic distribution leading to the same local electron densities is an acceptable solution for the structure determination with X-ray scattering.

3. Modeling the cubic α -(Al,Si)CuFe approximant phase

The previous refinement has been carried out from an initial structure that has been calculated from the quasicrystal using the perpendicular shear technique (Jarić & Qiu, 1990). Our quasicrystal model for i -AlCuFe is extracted from the work of Katz & Gratias (1995), on 6D representation of F -type icosahedral phases and modified according to the suggestions of Elser (1996, 1998) in the distribution of the atomic species. We will denote this model for short as the KGE model.

3.1. The starting icosahedral model

The icosahedral quasicrystal is defined in a 6D space by cutting along a 3D subspace denoted the parallel space \mathbf{E}_{\parallel} , a set of atomic surfaces (also called acceptance windows) that

are polyhedra parallel to the complementary orthogonal 3D space called \mathbf{E}_\perp and periodically distributed in the unit cells of an underlying 6D F (face-centered) lattice. The structure is characterized by the three main atomic surfaces shown in Fig. 1. Choosing as reference frame the primitive 6D lattice of length two times smaller than the one of the F lattice, we have:

(i) a large triacontahedron attached at the *even* nodes $(0, 0, 0, 0, 0, 0)$, hereafter denoted n ;

(ii) another large triacontahedron but truncated along a fivefold axis attached at the *odd* nodes $(1, 0, 0, 0, 0, 0)$, hereafter denoted n' ;

(iii) a small triacontahedron [deflated by $(1 + \tau)$ with respect to the previous ones] attached at the *odd* body centers $1/2(-1, 1, 1, 1, 1, -1)$, denoted bc .

The *even* body centers bc' are left empty. The atomic species distribute in these basic atomic surfaces according to Fe and Al on n , Al and Cu on n' and Cu on bc as shown in Fig. 2.

3.2. The shear method

To generate a (periodic) approximant, we apply a shear of the 6D lattice in \mathbf{E}_\perp so that the 6D lattice points $\lambda = (x_\parallel, x_\perp)$,

where x_\parallel and x_\perp denote the components of λ on respectively \mathbf{E}_\parallel and \mathbf{E}_\perp , transform according to:

$$x'_\parallel = x_\parallel, \quad x'_\perp = x_\perp - \varepsilon x_\parallel, \quad (1)$$

where ε is the 3×3 shear matrix defining the approximant and given by

$$\varepsilon = A_\perp A_\parallel^{-1}. \quad (2)$$

Here, A_\parallel and A_\perp designate the 3×3 matrices, the columns of which are respectively the parallel and perpendicular components of the three 6D lattice nodes that define the unit cell of the approximant.

The cubic stratum is obtained by choosing the unit cell $A = \{q, p, 0, -q, p, 0\}$, $B = \{p, 0, q, p, 0, -q\}$ and $C = \{0, q, p, 0, -q, p\}$, where p and q are coprime integers. In the present case, the structure corresponds to $p = q = 1$ and is thus called the '1/1' cubic approximant; the shear matrix reduces to

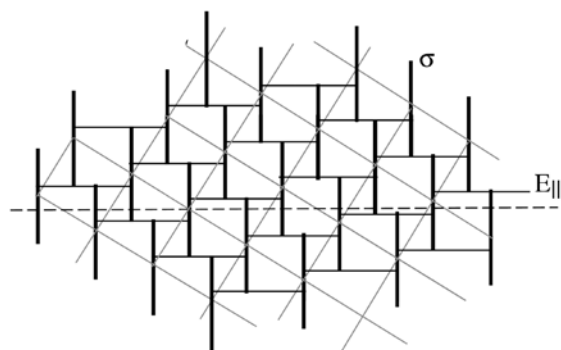
$$\varepsilon = -\tau^{-3} Id, \quad (3)$$

where Id designates the 3×3 identity matrix. The unit cell is given by $A = \alpha(2\tau^2, 0, 0)$ and cyclic permutations where α is the usual scaling constant (Cahn *et al.*, 1986), $\alpha = A_{6D}/[2(2 + \tau)]^{1/2}$. The lattice parameter is given by $a = 2\alpha\tau^2$.

A major difference between quasicrystals and approximants is that in the case of quasicrystals the projection in \mathbf{E}_\perp of the 6D lattice is uniformly dense in the perpendicular space, whereas in the case of periodic approximants these projections of the 6D lattice nodes collapse, after shear, into a discrete set of points (Gratias *et al.*, 1995; Quiquandon *et al.*, 1999), thus forming a 3D lattice in \mathbf{E}_\perp . Hence, the local isomorphism property of the quasicrystal disappears and *several* different approximant structures with different symmetry can be generated according to the location of the trace of \mathbf{E}_\parallel in \mathbf{E}_\perp . Only some specific cuts correspond to high-symmetry structures associated with locations in 6D corresponding to special points [called high-symmetry 'lock-in' points (Gratias *et al.*, 1995)] of the initial structure. This crucial point is exemplified in the simple 1D example shown in Fig. 3. At the top of the figure, the 2D representation of a 1D quasicrystal is given where the vertical lines are the atomic surfaces σ . At the bottom, a periodic approximant is obtained by a rational perpendicular shear of the 2D lattice. Two locations of the cut space \mathbf{E}_\parallel are drawn: the first one, denoted (1), passes through the origin of the 2D unit cell and is represented by the plain circles, the second one, denoted (2), passes through the body center of the 2D unit cell and is represented by the open circles. These two structures are different: for example, structure (1) is 'stable' with respect to perpendicular fluctuations of the cut whereas structure (2) generates numerous atomic jumps because, in that case, the cut passes exactly through several boundaries of the atomic surfaces.

For the icosahedral case, the projection of the 6D sheared lattice into \mathbf{E}_\perp leads to a 3D cubic lattice with a unit cell of parameter $a_\perp = \alpha(3 - \tau)$ along the three twofold axes common to the cubic $m\bar{3}$ and icosahedral point groups. Using

QUASICRYSTAL



APPROXIMANT

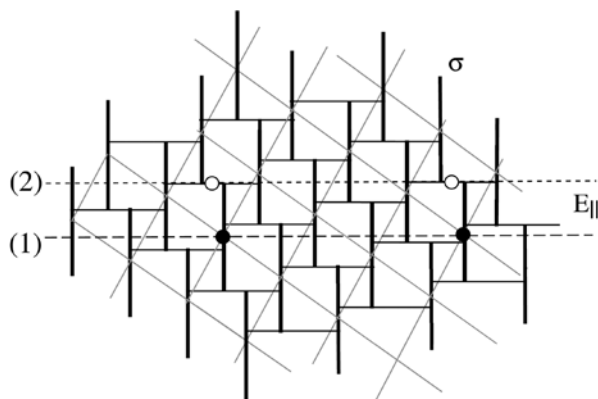


Figure 3
(Top) A 1D quasicrystal with its representation in 2D space. The vertical line segments parallel to \mathbf{E}_\perp represent the atomic surfaces denoted σ . Any horizontal cut leads to a locally isomorphic quasiperiodic sequence. (Bottom) Periodic 1D approximants are obtained after a rational shear along \mathbf{E}_\perp : different 1D structures are obtained according to where the cut space is located with respect to \mathbf{E}_\perp . Two of them with symmetry $\bar{1}$ are shown.

the Cahn *et al.* (1986) indexing scheme and, as demonstrated in Quiquandon *et al.* (1999), a 6D lattice point $(n_1, n_2, n_3, n_4, n_5, n_6)$ projects in \mathbf{E}_\perp after the shear associated with the p/q cubic stratum, on the node (U, V, W) given in cubic unit-cell coordinates by:

$$\begin{cases} U = p(n_4 - n_1) + q(n_2 + n_5), \\ V = p(n_6 - n_3) + q(n_1 + n_4), \\ W = p(n_5 - n_2) + q(n_3 + n_6), \end{cases} \quad (4)$$

where, here, $p = q = 1$. Thus, the 6D lattice points n and n' project in \mathbf{E}_\perp on 3D nodes with an *even* sum of coordinates $U + V + W$ and the points bc and bc' on nodes with an *odd* sum of coordinates. Therefore, 3D cuts passing through n and n' (as well as bc and bc') special points generate the same structure because the translation $(1, 1, 1, 0, 0, 0)$ that relates n to n' (and bc to bc') is the $(1, 1, 1)/2$ translation of the cubic unit cell in \mathbf{E}_\parallel : the two structures are identical but simply displaced by $(1, 1, 1)/2$. Hence, the projected 3D lattice in \mathbf{E}_\perp of the 6D F lattice is a 'double' f.c.c. lattice (NaCl type) of parameter $2a$ with n (n') sites at the vertices and bc (bc') sites at the body centers. Therefore, the cubic structures with point group $m\bar{3}$ (Quivy *et al.*, 1996; Yamada *et al.*, 1999; Hiraga *et al.*, 1997) are obtained only when the cut passes through two

different special points: the vertices n (n') or the body centers bc (bc'). This generates a total of only two possible cubic structures of point group $m\bar{3}$: the $n - 1/1$ cubic approximant and the $bc - 1/1$ cubic approximant. Building both structures, we observed that, contrarily to the n structure, the bc cubic structure could not lead to a satisfactory convergence and has therefore been discarded.

Beyond the symmetry aspect, a second strong geometrical constraint in the shear method is that the shear transformation should preserve the way nearby atomic surfaces connect so as to keep a constant topology (Oguey *et al.*, 1988; Kramer, 1988; Katz, 1988, 1989, 1990). This leads to distortion of the atomic surfaces and reshaping them after shear along the facets of the elementary 3D cube of the projected 6D lattice in \mathbf{E}_\perp as illustrated in Figs. 4 and 5. It must be noticed that, because of these distortions that generate numerous new facets, the vertices of which fall exactly on the nodes of the projected sheared lattice in \mathbf{E}_\perp , arbitrary decisions have to be taken for choosing which atomic species should be attached to those sites. We were guided in our choice by the overall stoichiometry and decided not to introduce partial occupancy factors for these 'critical points' in the initial structures. The resulting ideal structure of the $n - 1/1$ approximant is presented in Table 3.

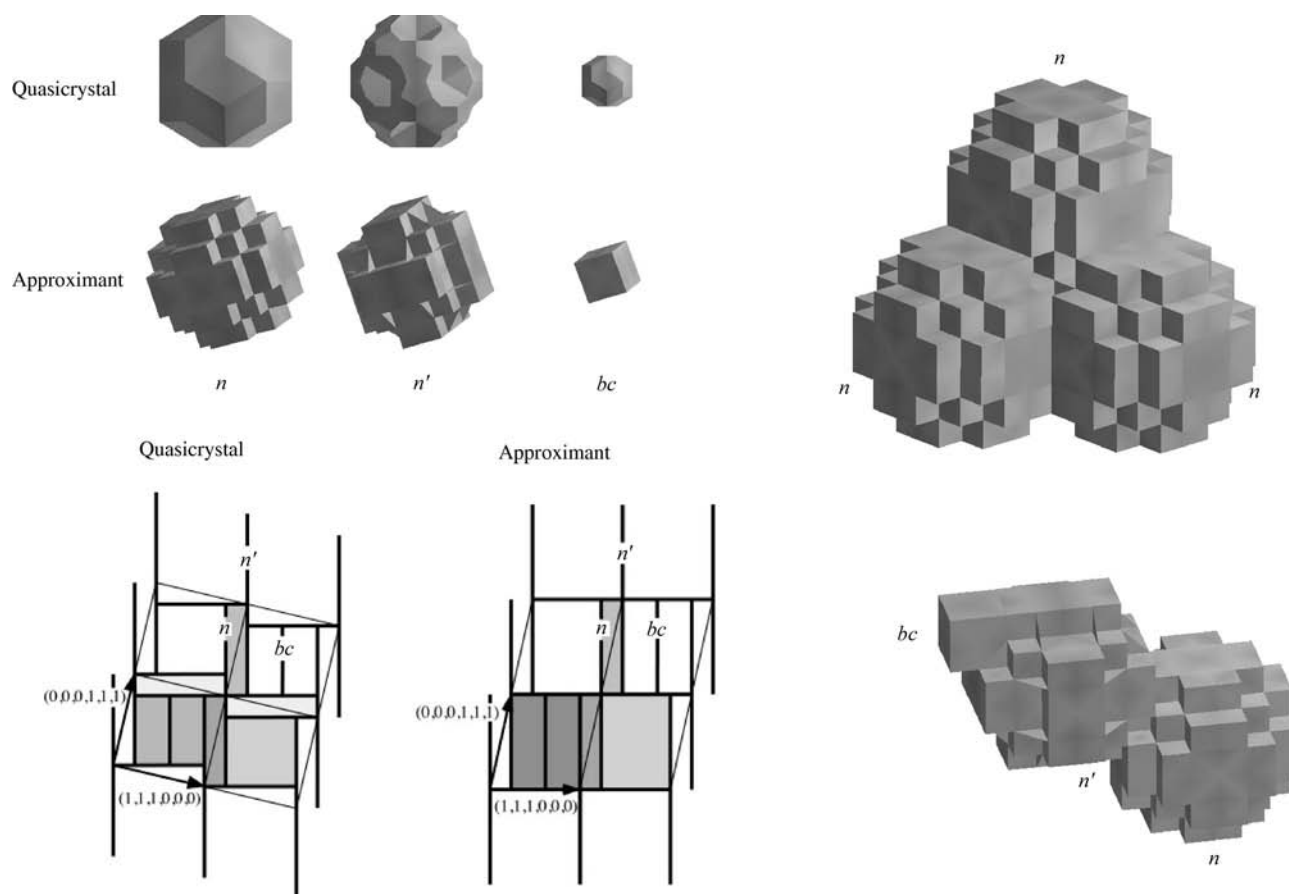


Figure 4

The basic atomic surfaces of the KGE model after the perpendicular shear corresponding to the $1/1$ cubic stratum. Transformation of the invariant 2D threefold planes from icosahedral to cubic symmetry. On the right, typical connections between the AS's observed in \mathbf{E}_\perp after shear.

Table 3

Ideal structure of the $n - 1/1$ approximant with space group $Pm\bar{3}$ after the shear process applied on the KGE model of the parent icosahedral phase AlCuFe $[(5 - 3\tau)/2 = 00729; (2 - \tau)/2 = 01910; (-3 + 2\tau)/2 = 01180; (-1 + \tau)/2 = 03090; 2 - \tau = 03820; (6 - 3\tau)/2 = 05729]$.

For consistency with Yamada *et al.* (1998, 1999) settings, the site n' has been chosen as origin.

Atom	Wyckoff position	x	y	z
Fe(1)	1	0	0	0
Fe(2)	12	$(5 - 3\tau)/2$	0	$(2 - \tau)/2$
Cu(3)	24	$(2 - \tau)/2$	$(-3 + 2\tau)/2$	$(-1 + \tau)/2$
Cu(4)	6	0	0	$2 - \tau$
Al(5)	12	0	$(2 - \tau)/2$	$(-1 + \tau)/2$
Fe(6)	1	$1/2$	$1/2$	$1/2$
Al(7)	12	$(6 - 3\tau)/2$	$1/2$	$(-1 + \tau)/2$
Al(8)	24	$(2 - \tau)/2$	$(-1 + \tau)/2$	$2 - \tau$
Al(9)	6	$(-3 + 2\tau)/2$	$1/2$	$1/2$
Cu(10)	12	$(2 - \tau)/2$	$1/2$	$(-1 + \tau)/2$
Cu(11)	6	0	$(-1 + \tau)/2$	$1/2$
Al(12)	12	0	$(6 - 3\tau)/2$	$(-1 + \tau)/2$
Al(13)	12	$(-3 + 2\tau)/2$	$(-3 + 2\tau)/2$	$1/2$

Table 4

Wyckoff positions ($\times 2$) for the basic orbits of the M (M') clusters in the $1/1$ cubic approximants; in each case, the origin is chosen at the center of the cluster.

Type	Symmetry	6D vector	Wyckoff position ($\times 2$)
$n - n'$	12	$[6, -3] : (1, 0, 0, -1, -1, 0)$	$(5 - 3\tau, 0, 2 - \tau)$
	8	$[6, -3] : (0, 1, -1, 1, 0, 0)$	$(-3 + 2\tau, -3 + 2\tau, 3 - 2\tau)$
$n - n'$	12	$[2, 1] : (0, 0, 1, 0, 0, 0)$	$(0, 2 - \tau, -1 + \tau)$
$n - n$	6	$[4, 0] : (0, 1, 0, 0, -1, 0)$	$(0, 0, 2(2 - \tau))$
	24	$[4, 0] : (0, 0, 0, 0, 1, 1)$	$(-1 + \tau, -2 + \tau, -3 + 2\tau)$
Extended			
$n - n'$	24	$[6, 1] : (0, 1, 0, 1, 0, 1)$	$(-3 + 2\tau, -3 + 2\tau, 1)$
	24	$[6, 1] : (1, 0, 0, -1, 0, -1)$	$(2(2 - \tau), 2 - \tau, 1 - \tau)$
	12	$[6, 1] : (0, 1, -1, 0, 0, -1)$	$(-1 + \tau, 0, 4 - 3\tau)$
Next ...			
$n - bc$	12	$[3, 3] : (1, 1, 1, -1, -1, 1)/2$	$(2 - \tau, 0, 1)$
	8	$[3, 3] : (1, 1, -1, 1, 1, -1)/2$	$(-1 + \tau, -1 + \tau, 1 - \tau)$
$n - n$	24	$[8, 0] : (1, 0, 1, -1, -1, 0)$	$(5 - 3\tau, 2 - \tau, 1)$
	24	$[8, 0] : (0, 1, -1, 1, 1, 0)$	$(-4 + 3\tau, -3 + 2\tau, 1 - \tau)$
	12	$[8, 0] : (1, -1, 0, -1, 1, 0)$	$(2(2 - \tau), 0, 2(-2 + \tau))$
$n' - bc$	12	$[3, 4] : (1, 1, 1, 1, -1, 1)/2$	$(0, -1 + \tau, 1)$
$n - n$	6	$[4, 4] : (0, 0, 1, 0, 0, 1)$	$(0, 0, 2(-1 + \tau))$
	24	$[4, 4] : (0, 1, 0, -1, 0, 0)$	$(1, 1 - \tau, 2 - \tau)$
...			

3.3. Bergman and Mackay clusters

Almost 95% of the atomic sites of the F -type icosahedral AlCuFe and AlPdMn alloys belong to a network of Bergman-type 33-atom B clusters (center + icosahedron + dodecahedron) located on the even nodes of a 3D Penrose tiling and connected by edges, complemented by Mackay-type 50-atom M clusters (center + partial dodecahedron + icosahedron + icosidodecahedron) as discussed by Elser (1996, 1998), Gratias, Quiquandon & Katz (2000) and Gratias, Puyraimond, Quiquandon & Katz (2000) (see Fig. 6). These clusters are generated by triacontahedral atomic surfaces in \mathbf{E}_\perp located at the special points of little group $m\bar{3}5$ of the 6D F lattice. With respect to the large triacontahedron located at n , these are:

(i) the even and odd nodes n and n' with a τ^{-3} scaled triacontahedron for the M and M' clusters;

(ii) the odd and even body centers bc and bc' with a τ^{-2} scaled triacontahedron for respectively the B and B' clusters.

An exhaustive study of how these clusters distribute in the icosahedral phases is to be found in Gratias, Puyraimond, Quiquandon & Katz (2000). With respect to the chemical decoration of the present model, it can be shown that:

(i) the B clusters distribute in 15 (slightly) different chemical configurations that correspond to the 15 kinds of $B-B$ edge-by-edge connections on the Penrose network;

(ii) the M clusters have one unique chemical configuration;

(iii) the M' clusters distribute on six different chemical configurations consistently with the geometry of the B -cluster network.

As will be discussed later, the triacontahedral atomic surfaces generating the B and M clusters transform in the $1/1$ cubic phase, respectively, into elementary cubes for the B 's and single points for the M 's. Thus, M clusters are generated only for the cubic structures corresponding to cuts that pass *exactly* through even nodes of the 3D projected lattice in \mathbf{E}_\perp , which is precisely the case we are interested in. The atomic positions

corresponding to the B and M clusters in the approximant are given in Tables 4 and 5, respectively.

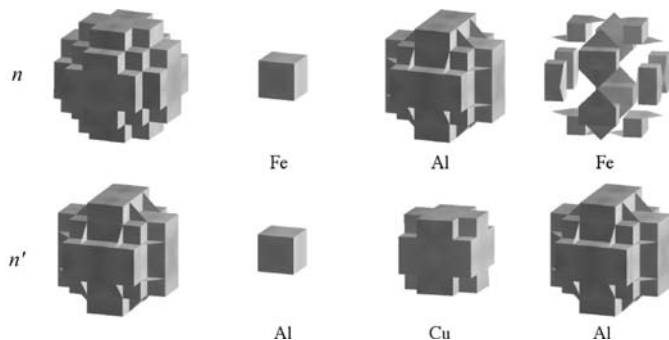


Figure 5
The atomic surfaces corresponding to the various atomic species of Fig. 2 after the perpendicular shear corresponding to the $1/1$ cubic stratum. After shear, the larger copper cell of the atomic surface n' is transformed to a point.

In the icosahedral case, B , B' , M and M' clusters can be extended to larger shells to form extended clusters called XM and XM' as recently introduced by Duneau (2000) in a search for a covering cluster of the F -icosahedral AlCuFe phase. These extended clusters of the icosahedral phase are shown in the first columns of Figs. 7 and 8.

In the case of the approximant phase, a similar analysis can be performed that leads to Figs. 7 [around the $(0, 0, 0)$ site] and 8 [around the $(1/2, 1/2, 1/2)$ site]. In both figures, the left column represents the polyhedra present in the extended clusters of the F -type icosahedral structure, XM and XM' , respectively. In the central column are the polyhedra obtained from the ideal approximant as described in Table 3 and the right column shows the corresponding polyhedra after final refinement. The final structure is very close to the initial theoretical structure with respect to both locations and chemical species except for two orbits, Al(2) and Al/Fe(6), that are expected to describe a partially filled dodecahedron

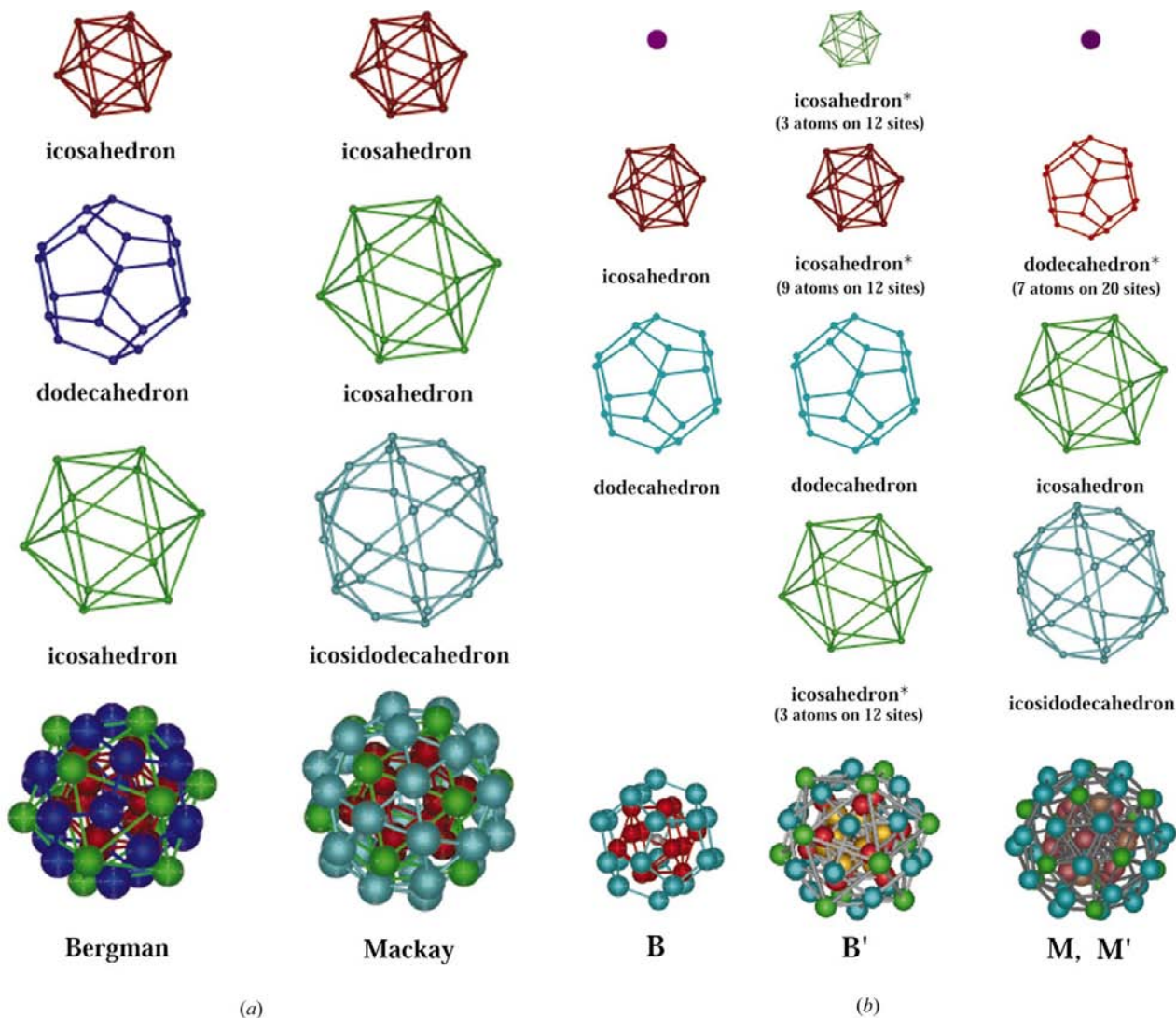


Figure 6
'Bergman' and 'Mackay' atomic clusters are found in complex intermetallic phases such as, respectively, T -(AlMgZn) (Bergman *et al.*, 1957) and α -(AlMnSi) (Cooper & Robinson, 1966; Guyot & Audier, 1985; Elser & Henley, 1985). The clusters B , B' and M/M' are found in F -type icosahedral quasicrystals and their approximants.

Table 5

Wyckoff positions ($\times 2$) for the basic orbits of the B (B') clusters in the 1/1 cubic approximants; the origin is chosen at the center of the cluster.

Type	Symmetry	6D vector	Wyckoff position ($\times 2$)
<i>B</i>			
$bc - n$	12	$[3, -1] : (1, 1, -1, 1, -1, 1)/2$	$(0, -3 + 2\tau, 2 - \tau)$
$bc - n'$	12	$[3, 0] : (-1, 1, 1, 1, 1, 1)/2$	$(-3 + 2\tau, 0, -1 + \tau)$
	8	$[3, 0] : (1, -1, 1, -1, 1, -1)/2$	$(2 - \tau, 2 - \tau, -2 + \tau)$
Extended			
$bc - n$	12	$[7, -1] : (1, -1, 1, 1, 1, 3)/2$	$(0, -3 + 2\tau, -4 + 3\tau)$
	24	$[7, -1] : (1, 1, 1, -3, -1, -1)/2$	$(2(2 - \tau), 3 - 2\tau, 2 - \tau)$
	24	$[7, -1] : (-1, 1, 1, -1, 1, -3)/2$	$(-1 + \tau, 5 - 3\tau, 1 - \tau)$
$bc - n'$	12	$[7, 0] : (-1, 1, 3, -1, -1, -1)/2$	$(0, 5 - 3\tau, 1)$
	24	$[7, 0] : (-1, 3, -1, 1, 1, 1)/2$	$(-4 + 3\tau, -2 + \tau, 2 - \tau)$
	24	$[7, 0] : (1, -1, -1, 1, 3, 1)/2$	$(-1 + \tau, -3 + 2\tau, 2(-2 + \tau))$
$bc - n$	12	$[3, 3] : (1, 1, 1, -1, -1, 1)/2$	$(2 - \tau, 0, 1)$
	8	$[3, 3] : (1, 1, -1, 1, 1, -1)/2$	$(-1 + \tau, -1 + \tau, 1 - \tau)$
$bc - n'$	12	$[3, 4] : (1, 1, 1, 1, -1, 1)/2$	$(0, -1 + \tau, 1)$
...			
<i>B'</i>			
$bc' - n$	12	$[7, -4] : (-1, -1, 3, -1, 1, -1)/2$	$(0, 5 - 3\tau, -3 + 2\tau)$
$bc' - n'$	12	$[3, -1] : (1, 1, -1, 1, -1, 1)/2$	$(0, -3 + 2\tau, 2 - \tau)$
$bc' - n$	12	$[3, 0] : (-1, 1, 1, 1, 1, 1)/2$	$(-3 + 2\tau, 0, -1 + \tau)$
	8	$[3, 0] : (1, -1, 1, -1, 1, -1)/2$	$(2 - \tau, 2 - \tau, -2 + \tau)$
$bc' - bc$	12	$[2, 1] : (0, 0, 1, 0, 0, 0)$	$(0, 2 - \tau, -1 + \tau)$
Extended			
$bc' - n'$	12	$[7, -1] : (1, -1, 1, 1, 1, 3)/2$	$(0, -3 + 2\tau, -4 + 3\tau)$
	24	$[7, -1] : (1, 1, 1, -3, -1, -1)/2$	$(2(2 - \tau), 3 - 2\tau, 2 - \tau)$
	24	$[7, -1] : (-1, 1, 1, -1, 1, -3)/2$	$(-1 + \tau, 5 - 3\tau, 1 - \tau)$
$bc' - n$	12	$[7, 0] : (-1, 1, 3, -1, -1, -1)/2$	$(0, 5 - 3\tau, 1)$
	24	$[7, 0] : (-1, 3, -1, 1, 1, 1)/2$	$(-4 + 3\tau, -2 + \tau, 2 - \tau)$
	24	$[7, 0] : (1, -1, -1, 1, 3, 1)/2$	$(-1 + \tau, -3 + 2\tau, 2(-2 + \tau))$
$bc' - n'$	12	$[3, 3] : (1, 1, 1, -1, -1, 1)/2$	$(2 - \tau, 0, 1)$
	8	$[3, 3] : (1, 1, -1, 1, 1, -1)/2$	$(-1 + \tau, -1 + \tau, 1 - \tau)$
$bc' - n$	12	$[3, 4] : (1, 1, 1, 1, -1, 1)/2$	$(0, -1 + \tau, 1)$
...			

but finally end up to be an almost full icosahedron. This important discrepancy will be discussed later.

Comparing the ideal 1/1 approximant structure and the icosahedral structure, we first observe that the clusters located at the $(0, 0, 0)$ and $(1/2, 1/2, 1/2)$ sites of this 1/1 approximant are similar to respectively the XM' and XM clusters of the quasicrystal, even at significantly large distances. Most of the polyhedra of the 1/1 approximant are polyhedra of the quasicrystal and in the same order in size with the following exceptions:

(i) for the XM' cluster [centered at $(0, 0, 0)$], the deltoid-hexecontahedron* (2) of the quasicrystal disappears in the approximant; *a contrario*, the deltoid-hexecontahedron* (1) that is partially occupied in the quasicrystal becomes fully occupied in the approximant; the icosahedron (2) is partially occupied in the quasicrystal and becomes fully occupied in the approximant;

(ii) for the XM cluster [centered at $(1/2, 1/2, 1/2)$], the deltoid-hexecontahedron* (1) of the quasicrystal changes its occupancy factor from the quasicrystal to the approximant.

Comparing now the ideal cubic structure obtained after shear and the refined structure, we observe the following features:

(i) the position Fe(6) $(1/2, 1/2, 1/2)$ center of the XM cluster of the ideal structure disappears in the refined structure;

(ii) as already mentioned, the positions Al(2) and Al/Fe(6) are partial dodecahedra in the ideal structure and transform into partial icosahedra in the refined structure;

(iii) for all others, the relaxation of positions between the ideal and refined structures is at most on the order of 3%.

(iv) the chemical decoration in both cases is globally similar with the exception of Al(2) in the final structure, which was expected to be Fe in the ideal structure and *a contrario* the final position Fe(5) that was initially Al in the ideal structure.

Fig. 9 shows the B and M clusters in both the ideal and the refined structures.

Concerning the cluster connections, it can first be noticed that they are similar between the approximant (ideal and refined) and the icosahedral structures. However, as expected because of the lowering of symmetry from icosahedral to cubic, new configurations appear in the cubic case that are not present in the icosahedral ideal structure especially for B - B and B - M connections. Indeed, the B clusters of the approximant overlap and new B - M intersections are observed that are not present in the icosahedral case. These topological differences are understandable by considering the underlying geometry of the acceptance windows (or cells) of the approximant in \mathbf{E}_\perp for the various B and M configurations as shown in Fig. 10 and Table 6.

The most important feature is that all cells in \mathbf{E}_\perp corresponding to the various M atomic shells reduce in points, edges or squares, *i.e.* in cells that are 0- (vertices), 1- (edges) or

2- (faces) dimensional and have zero volume. These kinds of low-dimension cells would be insignificant in the case of a general icosahedral cut but they are *strongly* pertinent in the approximant case because there the cut passes through special points precisely where these low-dimensional cells are located. This results in most of the atomic positions of the approximant being defined on the boundaries of *B* cells that are simultaneously the low-dimension cells of the *M* configurations. This generates new configurations where, for example, atoms of the *B* inner icosahedra belong to *two* *B* clusters because they issue from points that are located at the exact boundary between two *B* icosahedron cells. This is a highly specific geometrical situation where most of the atoms issue from critical boundary points as shown in Fig. 11 where all atomic positions of the




















ICOSAHEDRAL STRUCTURE	APPROXIMANT STRUCTURE	
	Polyhedra, located at the (0,0,0) site, corresponding to the M'-type cluster	
XM'	Ideal	Experimental
Center •	Center • Fe	Center • Fe
Dodecahedron* 0  7/20 0.25129 nm	Dodecahedron* 0 Fe 12  D d 0.25170 0.17963 0.29064	Icosahedron* 0 Al 10.70  D d 0.23556 0.24158 0.24924
Icosahedron 1  0.44651 nm	Icosahedron 1 Al 12  D d 0.44726 0.47028	Icosahedron 1 Fe 12  D d 0.46920 0.48922 0.49439
Icosidodecahedron 1  0.46949 nm	Icosidodecahedron 1 Cu 30  D d 0.47028 0.29064	Icosidodecahedron 1 Cu/Al 21.35/8.65  D d 0.46067 0.28522 0.45548 0.28852 0.27589
Deltoid-hexecontahedron* 1  53.52**/60 0.64791 nm	Deltoid-Hexecontahedron 1 Al 60  D d 0.64900 0.29064	Deltoid-Hexecontahedron 1 Al/Fe 58.80/1.20  D d 0.62819 0.27356 0.64964 0.32085 0.65221
Deltoid-hexecontahedron* 2  5.23**/60 0.66396 nm		
Icosahedron 2  8.76**/12 0.72247 nm	Icosahedron 2 Cu 12  D d 0.72368 0.76094	Icosahedron 2 Cu 12  D d 0.72520 0.76653 0.76152
Icosidodecahedron 2  0.75965 nm	Icosidodecahedron 2 Cu 30  D d 0.76094 0.47028	Icosidodecahedron 2 Cu/Al 23.45/6.55  D d 0.75296 0.46038 0.77063 0.44455 0.48631

Figure 7
The first column represents the polyhedra of the extended cluster *XM'* of the *F*-type icosahedral structure. In the other two columns are the polyhedra of the α -(Al,Si)CuFe structure, located at the (0,0,0) site, corresponding to the *M'*-type cluster. The distances *D* and *d* in nm correspond respectively to the distances from the center to the external shell and between the external shells [the 6D lattice parameter of the ideal model is $A = 0.63252$ nm deduced from the experimental 3D lattice parameter $a = 1.2312$ (2) nm]. The distances of the icosahedral structure correspond to the phase *i*-AlCuFe with a 6D lattice parameter $A = 0.63146$ nm. The symbols * and ** designate respectively a polyhedron partially filled and a mean value.

approximant are drawn in E_{\perp} . This explains why it is impossible for many Wyckoff positions to unambiguously define which atomic species they are associated with: they actually correspond to mixed occupancy of different atomic species.

All but two Wyckoff positions of the final structure fall on the cubic AS's (atomic surfaces) of the model once localized in E_{\perp} . These two sites Al(2) and Al/Fe(6), already mentioned throughout this paper, correspond to those theoretical partially occupied dodecahedral orbits that eventually transform into almost fully occupied icosahedra after the refinement process. These geometric discrepancies are to be considered together with the fact that the site Al(2) has an astonishing high Debye–Waller factor $B_{eq} = 13.9 \text{ \AA}^2$ (usually close to unity or less). A careful study of the vibrational ellipsoid of Al(2) presented in Fig. 12 shows that this site is associated with 12 very flat umbrella-like ellipsoids extending on the sphere containing the icosahedron as if the Al atoms were delocalized all over the surface of this sphere. In order to better reveal the differences between the refined structure and










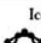




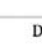



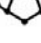


ICOSAHEDRAL STRUCTURE	APPROXIMANT STRUCTURE	
	Polyhedra, located at the (1/2,1/2,1/2) site, corresponding to the M-type cluster	
XM	Ideal	Experimental
Center •	Center • Fe	Center • Vacuum
Dodecahedron* 0  7/20 0.25129 nm	Dodecahedron* 0 Al 12  D d 0.25170 0.17963 0.29064	Icosahedron* 0 Al/Fe 10.30/1.70  D d 0.23907 0.24958 0.25182
Icosahedron 1  0.44651 nm	Icosahedron 1 Cu 12  D d 0.44726 0.47028	Icosahedron 1 Cu/Al 9.60/2.40  D d 0.46262 0.48693 0.48631
Icosidodecahedron 1  0.46949 nm	Icosidodecahedron 1 Al 30  D d 0.47028 0.29064	Icosidodecahedron 1 Al 30  D d 0.47401 0.28939 0.46847 0.28418 0.29409
Deltoid-hexecontahedron* 1  34.76**/60 0.64791 nm	Deltoid-hexecontahedron* 1 Cu 24  D d 0.64900 0.29064 0.47028	Deltoid-hexecontahedron* 1 Cu/Al 17.10/6.90  D d 0.65915 0.27589 0.49688
Dodecahedron* 1  7/20 0.65787 nm	Dodecahedron* 1 Cu 12  D d 0.65898 0.47028 0.76094	Dodecahedron* 1 Cu 12  D d 0.65805 0.46477 0.76152
Deltoid-hexecontahedron* 2  24/60 0.66396 nm	Deltoid-hexecontahedron* 2 Al 36  D d 0.66507 0.17963 0.29064 0.47028	Deltoid-hexecontahedron* 2 Al/Fe 34.80/1.20  D d 0.66379 0.24579 0.66724 0.45203
Icosidodecahedron 2  0.75965 nm	Icosidodecahedron 2 Al 30  D d 0.76094 0.47028	Icosidodecahedron 2 Fe/Al 24.00/6.00  D d 0.75729 0.45174 0.75035 0.43051 0.49439

Figure 8
The first column of the table represents the polyhedra of the extended cluster *XM* of the *F*-type icosahedral structure. In the other two columns are the polyhedra of the α -(Al,Si)CuFe structure, located at the (1/2, 1/2, 1/2) site, corresponding to the *M*-type cluster. The characteristics of this figure are identical to those of the previous one.

the actual structure, we calculated the reconstructed electronic Fourier difference map using the actual measured scattering amplitudes associated with the phases given by the model. This map is presented in Fig. 13 for the two cuts $z = 0$ and $z = 0.5$. The first column of this figure shows the experimental electron density ρ_{exp} , the second column shows the calculated electron density ρ_{cal} with the refined model and the last one shows the difference between them, $\rho_{\text{exp}} - \rho_{\text{cal}}$. It can be noticed that there is a globally good agreement between the experimental and the calculated maps that is confirmed by the difference map for which the scale of the intensity is one order of magnitude less than the one used in the two first columns. The ratio between the two scales of intensity is on the order of magnitude of the reliability factor, *i.e.* between 4 and 5%. The contrasts observed in the Fourier difference correspond to background noise and cannot be related to possibly missing atomic positions. The only slight differences that can be seen are to be found in the $z = 0$ map (see the enlargement inserts) around the Wyckoff position Al(2) that has this unusually large Debye–Waller factor. The delocalization seems even larger with a higher electron density in the experimental case than in the model enforcing the idea that this site is strongly

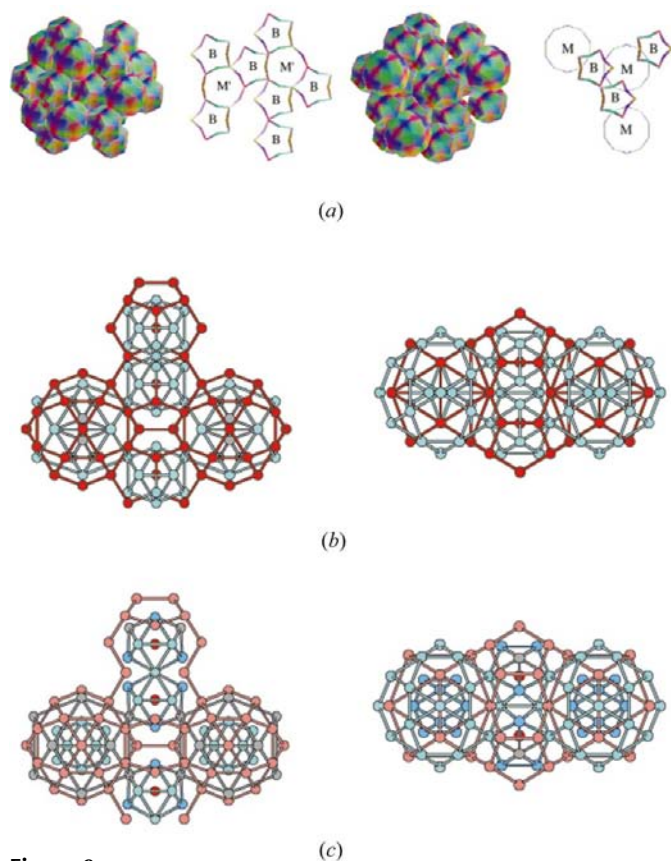


Figure 9 *B*- and *M*-cluster distributions (a) in the *F*-type icosahedral structure and in the $n - 1/1$ cubic approximant, (b) in the ideal structure, (c) in the refined structure. It can be observed that new connections occur between intersecting *B* clusters that are not present in the icosahedral structure (where *B* clusters connect only along the edges of their external dodecahedron).

topologically disordered. This is reminiscent of the thermal phason sites in quasicrystals.

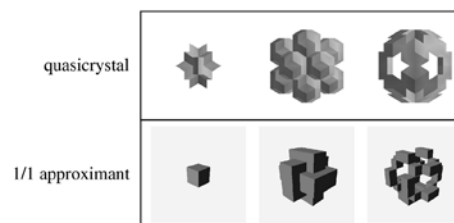
In any case, the presence of the questionable Al(2) site [and Al/Fe(6)] together with the absence of the theoretical site Fe(6) suggest that the *XM* and *XM'* clusters of the model should actually be closer to real Mackay clusters (Cooper & Robinson, 1966; Guyot & Audier, 1985; Elser & Henley, 1985) than they actually are as generated by the KGE model. This induces some subtle reshaping of the basic AS's of the model that can be sketched in two steps as described by Oguey *et al.* (1988):

(i) Removing the central atom [site Fe(6)] consists in excavating the large AS's by a τ^{-3} scaled small triacontahedron, thus leaving a central hole.

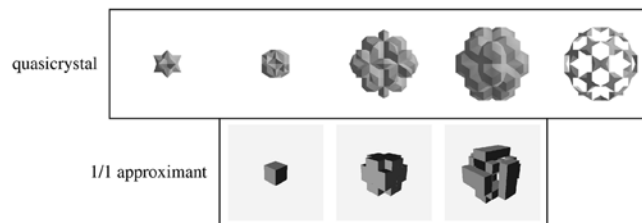
(ii) Replacing the partially occupied dodecahedron [sites Al(2) and/or Al/Fe(6)] by a full icosahedron is slightly more delicate: we add to the *bc* AS 12 small triacontahedra located on the centers of an icosahedron and remove on n' the cells that correspond to the partial dodecahedron. This generates an inner icosahedron in the physical space but with a too large radius which induces unacceptable distances with the atoms of

B-cluster cell decomposition

B-icosahedron



B-dodecahedron



M(*M'*)-cluster cell decomposition

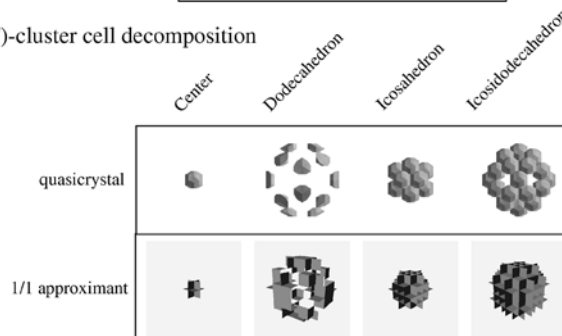


Figure 10

Comparison between the acceptance windows corresponding to the various atomic shells forming the *B* and *M* clusters for the icosahedral and 1/1 cubic cases. The acceptance windows defining the orbits of the *M* cluster, all based on the small triacontahedron, are represented in the 1/1 cubic case by points, edges and squares located or passing through special points.

the outer icosahedron. We therefore relax all these positions by a factor $(\tau^{-1} - 1/2)$ along the fivefold directions in \mathbf{E}_{\parallel} that shrinks the inner icosahedron to its actual size.

4. Conclusions

This study shows that there is a global good agreement between the experimental structure of an approximant and a theoretical model resulting from a perpendicular shear applied on the parent quasicrystalline structure. Moreover, it is possible to find the lock-in point that characterizes the approximant structure and therefore that determines the cluster type located at the cell origin. In this way, we can say that the 1/1 approximant α -(Al,Si)CuFe is a ‘Mackay-type’ approximant in the sense that, on the one hand, an M' cluster is located at the cell origin and an M cluster at the body center and, on the other hand, the B clusters – which are still present in the approximant – do not connect together the way they do

Table 6

Connections between the different cluster types and atomic positions with respect to the projected 6D lattice in \mathbf{E}_{\perp} after shear.

Atoms	AS	Atomic positions in \mathbf{E}_{\perp}	Local environments
Fe(1)	n'	(0,0,0)	Center M'
Al(2)	n	(0, -11, 7)	M' icosidodecahedron B dodecahedron (2)
Cu/Al(3)	n'	(1,1,2)	M' icosidodecahedron B dodecahedron (2)
Cu/Al(4)	n'	(0,0,2)	M' icosidodecahedron B dodecahedron (2)
Fe(5)	n	(0,1,1)	M' icosahedron B icosahedron
Al/Fe(6)	n'	(0, -11, -7)	M icosidodecahedron B icosahedron
Al(7)	n	(2,1,1)	M icosidodecahedron B icosahedron (2)
Al(8)	n	(0,0,2)	M icosidodecahedron B icosahedron (2)
Cu/Al(9)	n'	(0,1,1)	M icosahedron B dodecahedron (3)
Cu(10)	bc	(1,0,0)	Center B
Al/Fe(11)	n	(1,0,3)	B icosahedron
Al/Fe(12)	n	(2,2,0)	B icosahedron

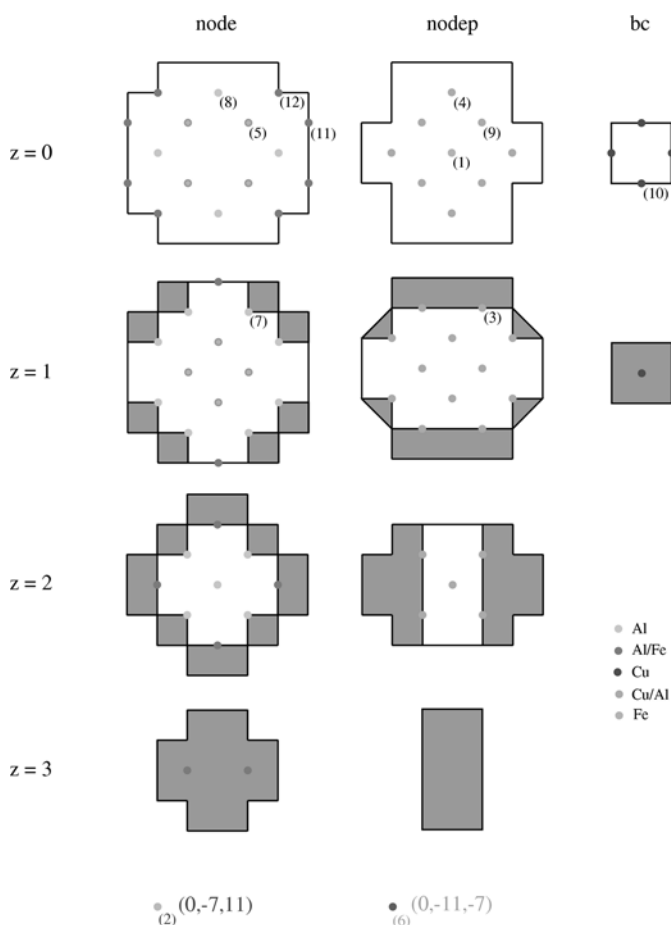


Figure 11

The Wyckoff positions of the final cubic structure as distributed in \mathbf{E}_{\perp} . They are almost on the vertices, edges or faces of B cells and on the low-dimension cells of M configurations. These result in atomic positions belonging simultaneously to various configurations and having mixed chemical occupancies. Two Wyckoff positions Al(2) and Al/Fe(6) fall outside the AS's of the model.

in the quasicrystal. Irrespective of small distortions, the major atomic clusters found in the approximant are those of the parent icosahedral structure, and we have shown that M , M' , B and B' clusters and their extended versions are present in both structures. It is quite interesting to notice that, even for such low-order approximants as the 1/1 studied here, their atomic local environments up to roughly 2 nm in diameter are almost identical to those of the parent quasicrystal. It is not very surprising that the electronic and transport properties are so close between the two phases.

Although the KGE model has been shown to be an acceptable starting point to investigate the approximant structure, we have noticed that it fails to reproduce the two Wyckoff positions corresponding to the inner icosahedra of the Mackay clusters out of which one has an unusually high

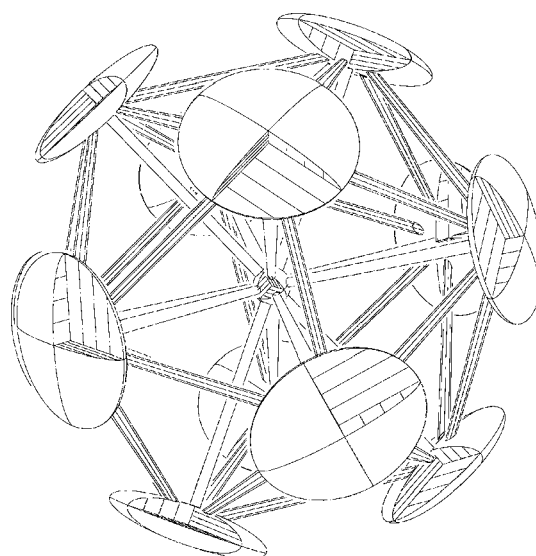


Figure 12

Vibrational ellipsoid of the Al(2) Wyckoff position.

Debye–Waller factor value [$B_{\text{eq}} = 13.9(7) \text{ \AA}^2$]. Attributing this exceptional value to a phason-like phenomenon in the approximant is plausible although we found no specific reason to select that position with respect to the many others in the structure that are also generated by points in \mathbf{E}_{\perp} located at the boundaries of some AS's. Another weakness in the present X-ray study is the relatively small diffraction contrast between the atomic species (Al/Si and Cu/Fe) that is not enough to unambiguously attribute the relative chemical occupancy of several mixed positions. Very recent results on similar samples obtained by V. Simonet and F. Hippert by neutron diffraction and EXAFS studies strongly suggest modifying

some occupancy factors of the present refined structure on at least one Wyckoff position. Beyond these specific problems of the fine chemistry distribution on the Wyckoff positions that are still open and should be solved through careful comparisons between neutron and X-ray data, the present study has demonstrated the validity of the perpendicular shear method to design prototypic ideal approximant structures from the parent quasicrystalline structure. A detailed description of the main atomic clusters has been performed showing the very close similarities between the local ordering of the approximant and the quasicrystal up to 2 nm; the approximant structure can reasonably be viewed as a periodic

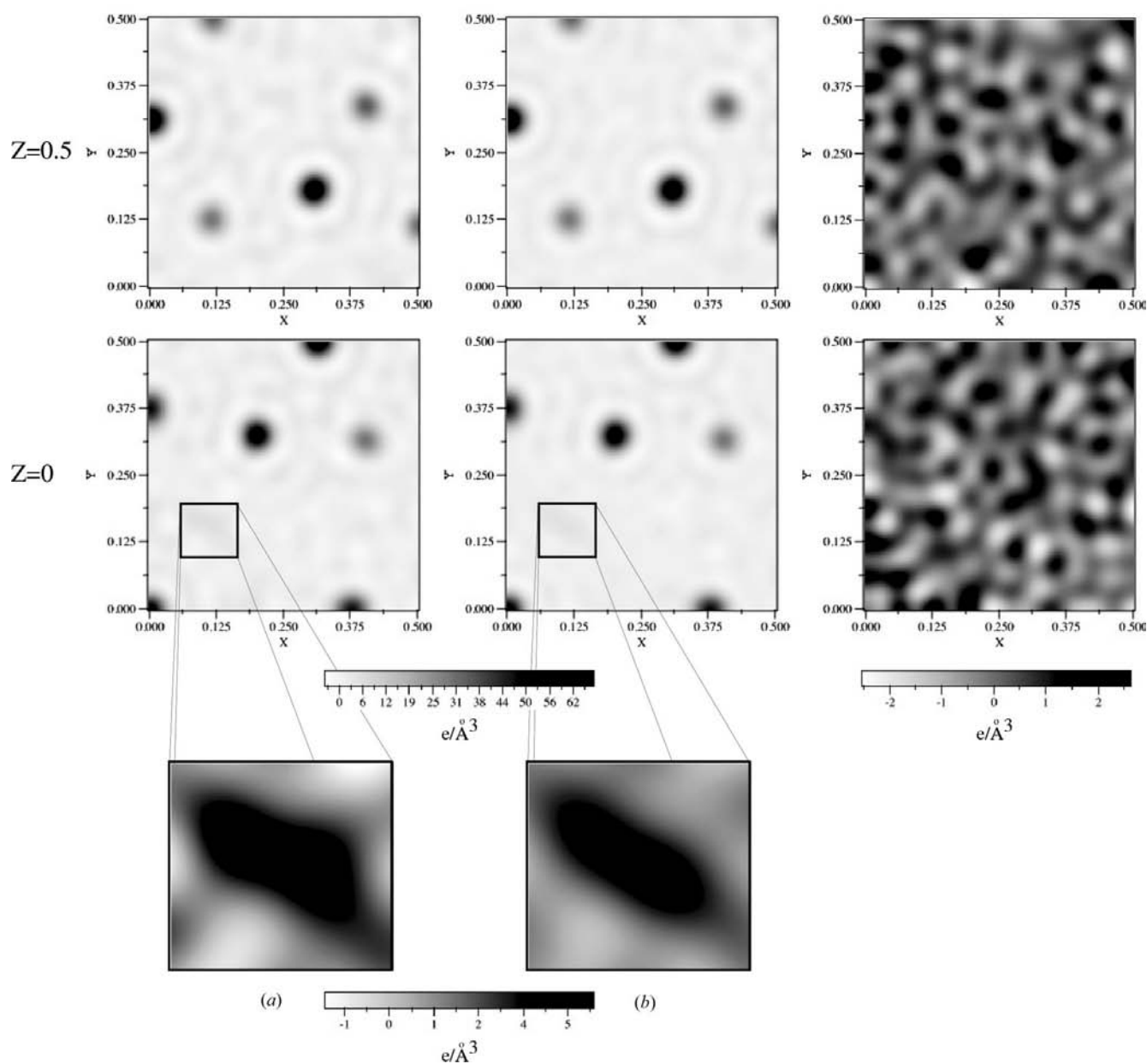


Figure 13

Electron-density maps of the α -AlSiCuFe phase for two different cuts $z = 0$ and $z = 0.5$. The first column shows the experimental electronic density ρ_{exp} , the second column shows the calculated electronic density ρ_{cal} and the last one shows the difference between the two, $\rho_{\text{exp}} - \rho_{\text{cal}}$. (a) and (b) represent the enlargement at $z = 0$ of the electron-density map around the Wyckoff position Al(2) for respectively the experimental case and the calculated case.

decoration of specific pieces of the quasicrystal developing on the same \mathbb{Z} -module.

We are very pleased to thank our colleagues V. Simonet and F. Hippert for having informed us of their very interesting neutron and EXAFS results prior to publication and the very fruitful discussions.

References

- Bergman, G., Waugh, L. T. & Pauling, L. (1957). *Acta Cryst.* **10**, 254–259.
- Cahn, J. W., Shechtman, D. & Gratias, D. (1986). *J. Mater. Res.* **1**, 13–26.
- Cooper, M. & Robinson, K. (1966). *Acta Cryst.* **20**, 614–617.
- Duneau, M. (2000). *Mater. Sci. Eng.* **294–296**, 192–198.
- Elser, V. (1996). *Philos. Mag. B*, **73**, 641.
- Elser, V. (1998). *Proceedings of the 6th International Conference on Quasicrystals*, edited by S. Takeuchi & T. Fujiwara, pp. 19–26. Singapore: World Scientific.
- Elser, V. & Henley, C. L. (1985). *Phys. Rev. Lett.* **55**, 2883–2886.
- Gratias, D., Katz, A. & Quiquandon, M. (1995). *J. Phys: Condens. Matter*, **7**, 9101–9125.
- Gratias, D., Puyraimond, F., Quiquandon, M. & Katz, A. (2000). *Phys. Rev. B*, **63**, 1–16.
- Gratias, D., Quiquandon, M. & Katz, A. (2000). *Quasicrystals, Current Topics*, edited by E. Belin-Ferré, C. Berger, M. Quiquandon & A. Sadoc, pp. 1–72. Singapore: World Scientific.
- Guyot, P. & Audier, M. (1985). *Philos. Mag. B*, **52**, L15–L19.
- Hiraga, K., Ohsuna, T. & Sugiyama, K. (1997). *J. Phys. Soc. Jpn*, **66**, 3700–3702.
- Izumi, F. & Ikeda, T. (2000). *Mater. Sci. Forum*, **321–324**, 198–203.
- Jarić, M. V. & Qiu, S.-Y. (1990). *Quasicrystals (12th Taniguchi Symposium)*, edited by T. Fujiwara & T. Ogawa, pp. 48–56. Berlin: Springer Verlag.
- Katz, A. (1988). *Commun. Math. Phys.* **118**, 263–288.
- Katz, A. (1989). *Introduction to the Mathematics of Quasicrystals, Aperiodic and Order*, Vol. 2, pp. 53–79. New York: Academic Press.
- Katz, A. (1990). *Proceedings of the Anniversary Adriatico Research Conference on Quasicrystals*, edited by M. Jarić & S. Lundqvist, pp. 200–217. Singapore: World Scientific.
- Katz, A. & Gratias, D. (1995). *Proceedings of the 5th International Conference on Quasicrystals*, edited by C. Janot & R. Mosseri, pp. 164–167. Singapore: World Scientific.
- Kramer, P. (1988). *J. Math. Phys.* **29**, 516–524.
- Oguey, C., Duneau, M. & Katz, A. (1988). *Commun. Math. Phys.* **118**, 99–118.
- Puyraimond, F., Tillard, M., Belin, C., Quiquandon, M., Gratias, D., Quivy, A. & Calvayrac, Y. (2001). *Ferroelectrics*, **250**, 281–284.
- Quiquandon, M., Katz, A., Puyraimond, F. & Gratias, D. (1999). *Acta Cryst.* **A55**, 975–983.
- Quivy, A., Quiquandon, M., Calvayrac, Y., Faudot, F., Gratias, D., Berger, C., Brand, R. A., Simonet, V. & Hippert, F. (1996). *J. Phys: Condens. Matter*, **8**, 4223–4234.
- Sheldrick, G. M. (1992). *Crystallographic Computing 5. From Chemistry to Biology*, edited by D. Moras, A. D. Podjarny & J. C. Thierry, pp. 145–157. IUCr/Oxford University Press.
- Sheldrick, G. M., Dauter, Z., Wilson, K. S., Hope, H. & Sieker, L. C. (1993). *Acta Cryst.* **D49**, 18–23.
- Sugiyama, K., Kaji, N., Hiraga, K. & Ishimasa, T. (1998). *Z. Kristallogr.* **213**, 168–173.
- Yamada, H., Iwakami, W., Takeuchi, T., Mizutani, U., Takata, M., Yamaguchi, S. & Matsuda, T. (1998). *Proceedings of the 6th International Conference on Quasicrystals*, edited by S. Takeuchi & T. Fujiwara, pp. 664–667. Singapore: World Scientific.
- Yamada, H., Takeuchi, T., Mizutani, U. & Tanaka, N. (1999). *Materials Research Society Symposium Proceedings*, Vol. 553, pp. 117–122. New York: Materials Research Society.